Ni *et al. BMC Medical Imaging* (2025) 25:79
https://doi.org/10.1186/s12880-025-01605-4

BMC Medical Imaging

RESEARCH Open Access

Magnetic resonance diffusion-derived vessel density (DDVD) as a valuable tissue perfusion biomarker for isocitrate dehydrogenase genotyping in diffuse gliomas

Chen-Xi Ni[1,5†], Ruo-Lan Lin[1,5†], Dian-Qi Yao[2], Fu-Zhao Ma[2], Yu-Ting Shi[1,5], Ying-Ying He[1,5], Yang Song[3], Guang Yang[4], Ri-Feng Jiang[1,5*] and Yì Xiáng J. Wáng[2*]

Abstract

Background Determining isocitrate dehydrogenase (IDH) mutation is crucial for glioma clinical management. MR diffusion-derived 'vessel density' (DDVD) offers non-invasive tissue perfusion evaluation within the tumor microenvironment. The study attempts to distinguish IDH genotypes of diffuse gliomas using DDVD in whole tumor parenchyma and its habitats.

Methods This study enrolled 63 patients with diffuse gliomas (30 IDH-mutant and 33 IDH-wildtype) who underwent diffusion-weighted (DW) imaging at 3T. $DDVD_{b0b10}$ was the signal difference between the $b=0$ and $b=10$ s/mm^2 DW images. $DDVD_{b0b10\_b10b20}$ is $DDVD_{b0b10}$ minus $DDVD_{b10b20}$. nDDVD was DDVD divided by signal intensity at $b=0$ s/mm^2 DW image. Correlations between DDVD metrics/intravoxel incoherent motion (IVIM) imaging metrics (*D* and *f*) and IDH genotypes/Ki-67 status were studied.

Results In tumor parenchyma, $DDVD_{b0b10\_b10b20}$ and $nDDVD_{b0b10\_b10b20}$ were lower, whereas *D* was higher in IDH-mutant gliomas [median (interquartile range): 12.76 (9.79–14.60); 15.14 (11.61–19.29); 1.31 (1.19–1.39)] compared to IDH-wildtype gliomas [14.48 (2.93–18.60), $p=0.008$; 20.55 (15.89–24.02), $p<0.001$; 1.16 (0.98–1.27), $p=0.003$]. Habitat analysis improved the diagnostic performance for IDH genotyping, with the highest AUC of 0.823 found for the $nDDVD_{b0b10\_b10b20}$ derived from the high $DDVD_{b0b10}$ value habitat. Diagnostic efficacy of the combined model of $nDDVD_{b0b10\_b10b20}$ with *D* was superior to that of combined model of *f* with *D*. The habitat model incorporating age, sex, and Karnofsky Performance Status further significantly enhanced the diagnostic efficacy, with an AUC reaching 0.979. Additionally, DDVD and *f* showed a positive correlation with Ki-67, while *D* exhibited a negative correlation with Ki-67 (all $p<0.05$).

[†]Chen-Xi Ni and Ruo-Lan Lin contributed equally to this work.

*Correspondence:
Ri-Feng Jiang
26630706@qq.com
Yì Xiáng J. Wáng
yixiang_wang@cuhk.edu.hk

Full list of author information is available at the end of the article

Conclusion DDVD, as a novel biomarker of microvascular perfusion, effectively differentiates IDH genotypes in gliomas. The habitat analysis improves the diagnostic accuracy for IDH genotyping.

Keywords Diffusion magnetic resonance imaging, Glioma, Isocitrate dehydrogenase, Ki-67

Background

Gliomas are among the most common and aggressive primary brain tumors, associated with poor prognosis. The molecular characterization has become critical in guiding treatment strategies and predicting outcomes for glioma patients. Based on the molecular characteristics, particularly isocitrate dehydrogenase (IDH) status, adult-type diffuse gliomas are currently categorized into glioblastoma (IDH-wildtype), astrocytoma (IDH-mutant), and oligodendroglioma (IDH-mutant and 1p/19q-codeleted) [1]. IDH mutations are associated with better prognosis and therapeutic responses compared to IDH-wildtype gliomas. Accurate and non-invasive methods for determining IDH status are highly valuable in clinical practice.

The apparent diffusion coefficient (ADC), derived from diffusion-weighted imaging (DWI), is a metric for assessing tissue cellularity and has been attempted to assess tumor grades and IDH genotypes of gliomas [2]. However, DWI has certain limitations due to the use of a monoexponential model. ADC values are influenced not only by molecular diffusion but also by perfusion effects and T2 effect which can lead to overestimation or underestimation of true diffusion [3, 4]. This is particularly relevant in gliomas, which are known for their heterogeneous vascularity. The intravoxel incoherent motion (IVIM) imaging yields metrics of the slow diffusion coefficient (D_{slow} or D), the fast perfusion-related diffusion coefficient (D_{fast} or D^*) and perfusion fraction (*PF or f*). IVIM imaging has been attempted to assess tumor grading, IDH mutation analysis, cellular proliferation and predicting survival of glioma patients [3, 5–7]. However, the clinical application of IVIM still has great challenges. IVIM's perfusion quantification is often impeded by noise sensitivity and the instability of data fitting process [8, 9]. Moreover, the perfusion and diffusion components in IVIM are noted to be mutually constrained [10, 11], and T2 shortening will lead to artificial elevation of f and D_{fast} measurement [12, 13].

Recently, magnetic resonance diffusion-derived 'vessel density' (DDVD), a functional parameter indicative of microvascular perfusion, has been proposed [14]. In vivo blood vessels show high signal when there is no motion probing gradient ($b = 0$ s/mm^2) and low signal when even very low b-values (such as $b = 1$, $b = 2$) are applied. For spin-echo type EPI sequence, the second motion probing gradient after the 180-degree RF pulse could not fully refocus the flowing spins in vessel and micro-vessels after being de-phased by the first motion probing gradient before the 180-degree RF pulse. The analysis of DDVD requires only two b-values, with a significantly shorter scanning time than contrast enhanced CT/MRI while without the need of a contrast agent injection [15–21]. Huang et al. [16] showed that DDVD analysis demonstrates liver parenchyma has an age-dependent decrease of micro-perfusion in healthy women. This agrees with the known physiological age-dependent reduction in liver blood flow. He et al. [17]. and Li et al. [18] reported that analysis of placenta DDVD allows excellent separation of normal and early pre-eclampsia pregnancies. Lu et al. [19]. reported that placenta regional DDVD is significantly higher in pregnant women with placenta accreta spectrum disorders than women with normal placenta. Hu et al. [20]. described that liver hemangiomas can be mostly differentiated from liver mass-forming lesions (hepatocellular carcinomas and focal nodular hyperplasia) solely based on DDVD pixel map. Chen et al. [21]. reported proof-of-concept case that DDVD pixelwise map assessments of brain ischemic area/volume are consistent with perfusion CT results, and a combination of DDVD pixelwise map and high b-value DW image identify the exitance and the size of a penumbra. As absolute MR signal intensity is influenced by various factors, including B0/B1 spatial inhomogeneity, coil loading, receiver gain, etc., the ratio of a lesion to its adjacent native tissue can be used to minimize these scaling factors. Li et al. [12] reported that ratio of HCC DDVD to background liver DDVD concur with earlier dynamic contrast enhanced CT results [22, 23]. Lu et al. [24] reported earlier clinical grades rectal carcinoma had a higher ratio of tumor DDVD to tumor-free rectal wall DDVD than those of the advanced clinical grades. This is consistent with the biology of rectal carcinoma [25, 26]. Recently, Wang et al. [27]. described that endometrial carcinoma with Ki-67 high-proliferation or aggressive histological type had higher DDVD value than those with Ki-67 low-proliferation or non-aggressive histological type. ROC curve analysis shows AUC of 0.873 for distinguishing between Ki-67 low- and high-expression, and AUC of 0.771 for distinguishing between non- aggressive and aggressive histological types. DDVD also readily provides in vivo perfusion information for parotid gland tumors [21, 28].

Although research on DDVD has shown promising applications in abdominal organs and in brain ischemic stroke, its potential in brain gliomas has not been explored. Given that more angiogenesis is found in IDH-wildtype gliomas, particularly glioblastomas, compared

to IDH-mutant gliomas [29, 30], we hypothesize that DDVD can serve as a useful biomarker for IDH genotyping. The term "tumor habitat" denotes the distinctive spatial microenvironment that arises from the interaction between tumor cells and their surroundings as they adapt to various survival pressures [31]. Intra-tumoral spatial heterogeneity is a well-established phenomenon in gliomas, particularly in glioblastoma at both genomic and transcriptomic levels [32, 33]. Recently, habitat analysis employed various imaging modalities to segment the tumor into distinct spatial compartments [34]. By integrating habitat analysis with DDVD, it may be possible to achieve more precise and robust differentiation of IDH genotypes.

Methods

Patients and clinical information

Between March 2019 and July 2023, this prospective study enrolled 106 glioma suspects. Ethical approval was granted by the local Ethics Committee, and all participants provided informed consent. Exclusion criteria included incomplete or poor-quality imaging (e.g., significant artifacts or head motion), absence of surgery or biopsy, non-glioma histological diagnoses, inadequate tissue for genetic analysis, and prior glioma therapy. The final study cohort comprised 63 patients (33 males, 30 females) (Fig. 1). Demographic and clinical data such as sex, age, and recurrence rates were documented. Clinical evaluations included the assessment of Karnofsky Performance Status (KPS).

MRI data acquisition

Structural MRI and multi-b-value DWI were performed on a 3.0-T system (MAGNETOM Prisma, Siemens Healthcare) utilizing a 64-channel head coil. The structural MRI included pre-contrast sagittal T1-weighted magnetization prepared rapid gradient echo sequence (T1-MPRAGE), axial T2-weighted (T2W) fast spin-echo (FSE) images, axial fluid-attenuated inversion recovery (FLAIR) T2W images, gradient echo (GRE) sequence, and post-contrast FLAIR T1W images in axial, sagittal, and coronal planes. For DWI, a single-shot echo planer imaging (SE-EPI) sequence was applied with parameters: repetition time, 2,000 ms, echo time, 69 ms; slice thickness, 5 mm; gap, 1 mm; field of view, 23 cm × 23 cm; acquisition matrix, 128 × 128; GRAPPA, 2; slice acceleration factor, 2; and pixel bandwidth, 2055 Hz/pixel. The acquisition encompassed 16 b-values (0, 10, 20, 40, 60, 80, 100, 120, 140, 160, 180, 200, 300, 500, 750 and 1,000 s/mm^2) with a single number of excitation (NEX), totaling a scan duration of 2 min 09 s.

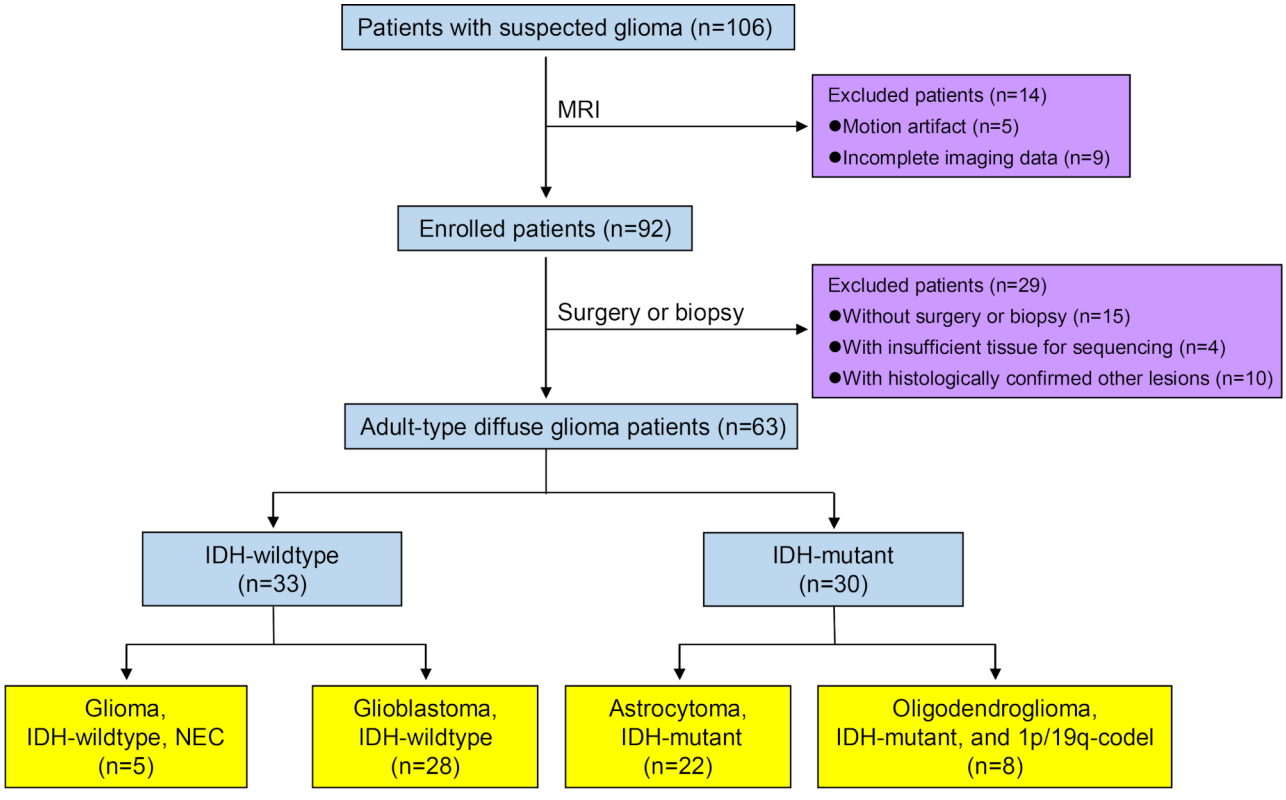

Fig. 1 Screening process for patients with glioma. IDH = isocitrate dehydrogenase, 1p/19q-codel = synchronous deletion of the short arm of chromosome 1 and long arm of chromosome 19, NEC = not elsewhere classified

DWI processing and analysis

All diffusion-weighted images were subjected to denoising and motion correction using QSIprep (https://github.com/PennLINC/qsiprep). DDVD pixelwise maps were computed using the following Eqs [20, 28].:

$$DDVD_{b0b10} = S_{b0}/ROI_{area\_b0} - Sb10/ROI_{area\_b10} \quad (au/pixel) \quad (1)$$

$$DDVD_{b0b10\_b10b20} = \left(S_{b0}/ROI_{area\_b0} - S_{b10}/ROI_{area\_b10}\right) - \left(S_{b10}/ROI_{area\_b10} - S_{b20}/ROI_{area\_b20}\right) \quad (au/pixel) \quad (2)$$

$$nDDVD = DDVD/\left(S_{b0}/ROI_{area\_b0}\right) \quad (\%) \quad (3)$$

Where S_{b0}, S_{b10} and S_{b20} refers to the sum of signals within the selected region of interest (ROI) on $b = 0$, 10 and 20 s/mm^2 images, respectively. ROI_{area_b0}, ROI_{area_b10}, and ROI_{area_b20} refer to the ROI area (unit in pixel) on $b = 0$, 10 and 20 s/mm^2 images. $DDVD_{b0b10}$ denotes the average signal intensity difference between $b = 0$ s/mm^2 and $b = 10$ s/mm^2, per unit area or per pixel. $DDVD_{b0b10\_b10b20}$ was to address the issue of signal decay associated with diffusion. By subtracting the b10b20 element from b0b10, $DDVD_{b0b10\_b10b20}$ reduces the diffusion component inherent in $DDVD_{b0b10}$, leading to a more precise interpretation of the tissue micro-perfusion [28]. Furthermore, nDDVD represents the normalized signal intensity difference adjusted by the mean signal intensity at $b = 0$ s/mm^2 [14].

IVIM parameter maps including D and f were also computed by MITK Diffusion (https://github.com/MIC-DKFZ/MITK-Diffusion) using a segmented fitting approach with threshold b-value of 170 s/mm^2 according to the biexponential IVIM model as follows:

$$S_b/S_{b0} = f.exp\left(-bD^*\right) + (1-f).\exp\left(-bD\right) \quad (4)$$

where S_{b0} and S_b are the diffusion-weighted signal intensities for $b = 0$ s/mm^2 and a non-zero b value, respectively.

ROI placement and habitat analysis

Structural MR images were registered to the $b = 0$ images using SPM12 (Wellcome Centre for Human Neuroimaging; http://www.fil.ion.ucl.ac.uk/spm/). ROIs over the whole tumor parenchyma (TP) were delineated on all tumor slices using ImageJ (version 1.49o, NIH; https://imagej.nih.gov/ij/) by two neuroradiologists (R.F.J. and Y.F.S.) who were blinded to histological results. The enhanced TP was outlined using transverse gadolinium-enhanced T1-weighted images when clear enhancement region was present, while for non-enhanced tumors, the TP was identified on transverse FLAIR T2W images or T2W images. Identifiable necrotic areas, cysts, edema, and calcifications were excluded from the ROIs. Figure 2 illustrates ROI delineation in sample cases for each tumor type.

Habitat analysis was conducted on the whole TP ROI using nnFAE (an in-house Python-based software). $DDVD_{b0b10\_b10b20}$, $DDVD_{b0b10}$, $nDDVD_{b0b10\_b10b20}$, $nDDVD_{b0b10}$, D and f maps were respectively selected as the primary quantitative parameters for habitat analysis. We applied the Otsu threshold method to classify the voxels of the whole TP into high- and low-value regions across the entire cohort for each parameter map. The threshold was iteratively set to minimize intra-class and maximize inter-class variance. The resulting subregions from each parameter map were amalgamated to yield two distinct final subregions, known as habitats: low value region (mask1) and high value region (mask2). Subsequently, the average values of the selected parameters in the whole TP and the identified habitats were computed for further evaluation.

Molecular and genetic detection of adult-type diffuse glioma

Molecular profiling was conducted via multiplexed polymerase chain reaction (PCR) coupled with next-generation sequencing to elucidate key genetic characteristics. Targeted detection of single-nucleotide variants (SNVs) identified mutations at IDH1^{R132}, IDH2^{R172}, TERT C228T, and TERT C250T. Copy number variation (CNV) analysis pinpointed 1p/19q co-deletion, chromosome 10 loss, and chromosome 7 gain. Quantitative real-time PCR evaluated EGFRvIII amplification. The presence of an IDH1 ^{R132} or IDH2 ^{R172} mutation classified the glioma as IDH-mutant; absence indicated an IDH-wildtype diagnosis. Patients were grouped according to IDH genotypes (IDH-wildtype or IDH-mutant), and were subsequently placed in three subtypes according to WHO CNS5 subtype criteria [1]. The Envision technique was used for immunohistochemical staining. The Ki-67 labeling index (LI) was defined as the percentage of nuclear staining-positive cells with any intensity in the high-density staining area in the total cells.

Statistical analysis

Statistical analysis was executed using SPSS (version 27, IBM Corp.). Intraclass correlation coefficient (ICC) verified inter-rater reliability. Group comparisons were conducted utilizing the Kruskal-Wallis test for continuous variables (age, KPS, Ki-67 LI) and Fisher's exact test for categorical outcomes (sex and recurrence rate). Mann-Whitney U tests were performed to compare differences in each metric between IDH genotypes. Binary Logistic Regression synthesized features into predictive equations for IDH genotype identification. ROC curve and AUC were used to assess diagnostic performance. AUCs were compared using the DeLong test. Spearman's correlation

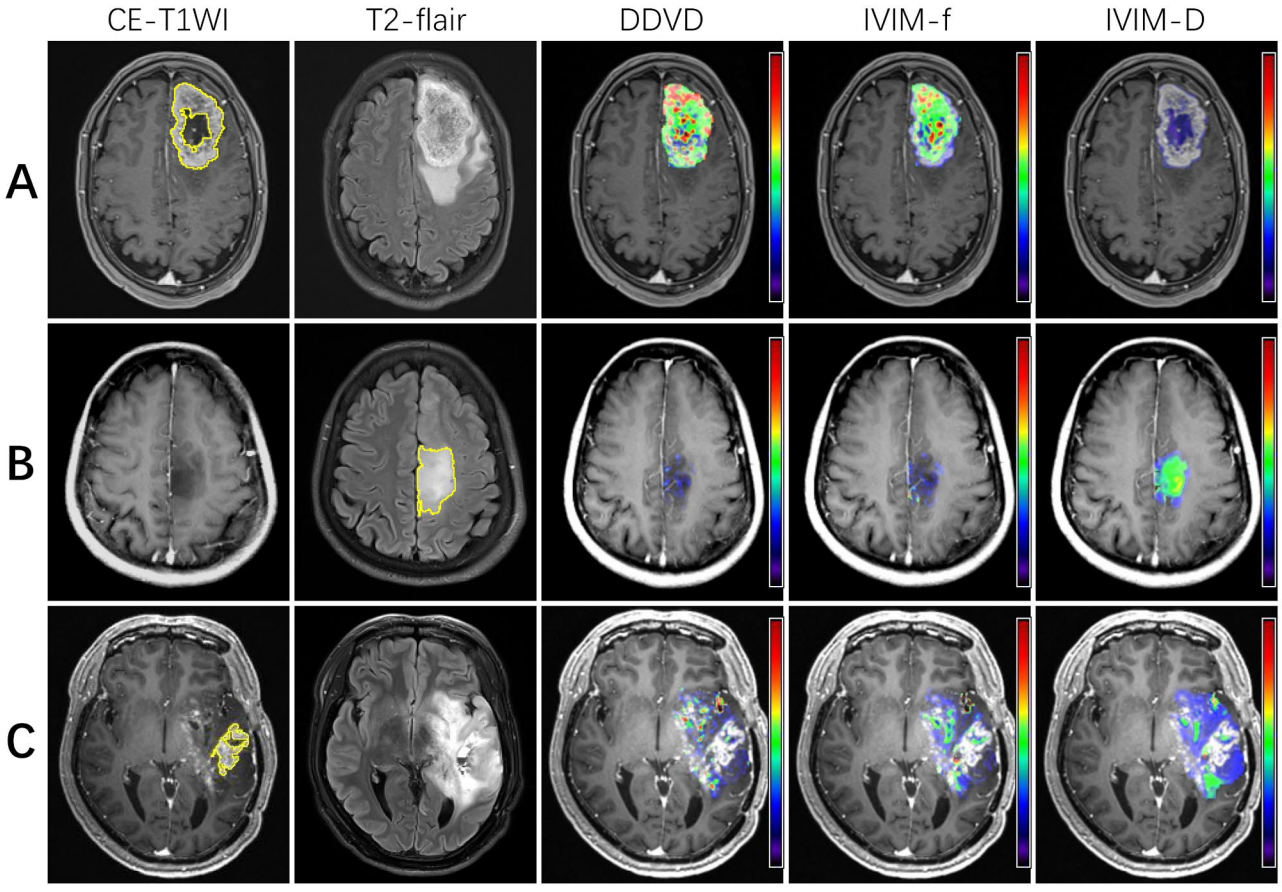

Fig. 2 Examples of ROI delineation and representative cases of gliomas. (**A**) A 73-year-old female patient with glioblastoma, IDH-wildtype in the left frontal lobe showing high $DDVD_{b0b10\_b10b20}$ value, high f value and low D value; (**B**) a 53-year-old female patient with astrocytoma, IDH-mutant (grade 2) in the left frontal lobe showing low $DDVD_{b0b10}$ value, low *f* value and high *D* value; and (**C**) a 31-year-old male patient with astrocytoma, IDH-mutant (grade 4) in the left temporal lobe showing low $DDVD_{b0b10}$ value, low *f* value and moderate (*D*) value. ROI = region of interest, IDH = isocitrate dehydrogenase, DDVD = diffusion-derived vessel density, IVIM = intravoxel incoherent motion

examined Ki-67 LI correlations with metrics. The *p* values were adjusted for multiple comparisons using the Benjamini-Hochberg method.

Results

Participant characteristics

Patient demographics for the 63 subjects are detailed in Table 1. Of the 33 with IDH-wildtype glioma, 28 were glioblastoma and 5 were IDH-wildtype glioma, not elsewhere classified (NEC). The 30 with IDH-mutant glioma comprised 22 astrocytomas and 8 oligodendrogliomas. There were no significant differences in sex and recurrence rate across the groups ($p = 0.469$ and 0.845). However, age, KPS, and Ki-67 LI varied significantly ($p < 0.001$, $p = 0.038$, and $p = 0.002$), with patients of IDH-wildtype glioma exhibiting older age, reduced KPS, and elevated Ki-67 LI.

Comparisons of DDVD and IVIM values among different tumor groups

The inter-observer reproducibility of measurements in 45 randomly selected patients is described in Supplementary Table S1 (for whole TP) and Supplementary Table S2 (for habitats analysis). The ICCs ranged between 0.813 and 0.958 for the whole TP and between 0.578 and 0.980 for the tumor habitats, indicating good to excellent reproducibility between radiologists. The measurement data from R.F.J were used for subsequent statistical analysis. Comparisons of DDVD and IVIM values between IDH genotypes and between tumor subtypes are listed in Table 2 and visualized in Fig. 3. Compared with IDH-mutant gliomas, $DDVD_{b0b10\_b10b20}$ and $nDDVD_{b0b10\_b10b20}$ of the whole TP were significantly higher in IDH-wildtype gliomas ($p = 0.008$ and < 0.001, respectively), whereas *D* was significantly lower ($p = 0.003$). In contrast, no significant differences were found for the $DDVD_{b0b10}$, $nDDVD_{b0b10}$ and *f* between two groups ($p = 0.296$, 0.080 and 0.080, respectively). Compared with astrocytoma,

Table 1 Participant demographic, clinical, and pathological characteristics

Characteristic	IDH-wildtype ($n=33$)	IDH-mutant ($n=30$)		p
		1p19q-intact ($n=22$)	1p19q-codel ($n=8$)	
Age (years)	57.5 (50–64)	36 (32–46)	45 (35–47)	$<0.001^{**}$
Sex (male/female)	17/16	12/10	4/4	0.469
KPS	80 (50–90)	80 (70–90)	90 (90–90)	0.038^{*}
Recurrent/primary glioma	7/26	6/16	2/6	0.845
WHO CNS5 subtype				
Glioblastoma	28	NA	NA	NA
Astrocytoma (grade 2/3/4)	NA	13/4/5	NA	NA
Oligodendroglioma (grade 2/3)	NA	NA	6/2	NA
Ki-67 LI (%)	32.5 (12.5–50)	10 (5–30)	5 (4.5–10)	0.002^{**}

Values are presented as number or median (interquartile range). $^{*}p<0.05$ and $^{**}p<0.01$. IDH = isocitrate dehydrogenase, 1p19q-codel = synchronous deletion of the short arm of chromosome 1 and long arm of chromosome 19, KPS = Karnofsky performance status, WHO CNS5 = fifth edition of the World Health Organization Classification of Tumors of the Central Nervous System, NA = not applicable, Ki-67 LI = Ki-67 labeling index

$DDVD_{b0b10\_b10b20}$ and $nDDVD_{b0b10\_b10b20}$ were significantly higher ($p=0.014$ and 0.006), whereas D was significantly lower in glioblastoma ($p=0.014$). In contrast, no significant differences were found for the other comparisons among different tumor subtypes ($p>0.05$ for all).

Diagnostic performances of DDVD and IVIM values for IDH genotyping

The AUC, sensitivity and specificity of the DDVD and IVIM metric values when separating IDH genotypes are listed in Table 3. The ROC curves are depicted in Fig. 4. The AUCs of the metric values derived from the whole TP ranged from 0.577 to 0.763. The $nDDVD_{b0b10\_b10b20}$ value demonstrated the best diagnostic performance in distinguishing IDH-mutant gliomas from IDH-wildtype gliomas; with an AUC and 95% confidence interval (CI) of 0.763 (0.644–0.881), a sensitivity of 90.00%, and a specificity of 57.58%. The D and $DDVD_{b0b10\_b10b20}$ values also showed moderate diagnostic performance, with AUCs of 0.746 and 0.709, respectively.

The segmentation thresholds of habitat analysis using Otsu threshold method were 15.095 for $DDVD_{b0b10\_b10b20}$ map, 25.529 for $DDVD_{b0b10}$ map, 20.308×10^{-3} for $nDDVD_{b0b10\_b10b20}$ map, 22.385×10^{-3} for $nDDVD_{b0b10}$ map, 1.377×10^{-3} for D map and 0.068 for f map. After habitat analysis, the diagnostic performance of each metric value for IDH genotyping showed varying degrees of improvement. The most notable improvements were observed in the metric values derived from the high-value habitat segmented based on the $DDVD_{b0b10}$ map ($DDVD_{b0b10}$, mask2) and the low-value habitat segmented based on the D map (D, mask1). The best AUCs of the metric values derived from habitats ranged from 0.731 to 0.823, as shown in Table 3.

Logistic regression models in identifying IDH genotypes

Binary logistic regression modeling further enhanced the diagnostic performance for IDH genotyping, as shown in Table 4. For whole TP features, the combined model of $nDDVD_{b0b10\_b10b20}$ and D (model1) achieved an AUC (95% CI) of 0.812 (0.708–0.917), higher than the combined model of f and D (model2), which had an AUC (95% CI) of 0.774 (0.656–0.892). Similarly, for habitat features, the combined model of $nDDVD_{b0b10\_b10b20}$ and D (model3) achieved an AUC (95% CI) of 0.866 (0.777–0.954), higher than the combined model of f and D (model4), with an AUC (95% CI) of 0.828 (0.721–0.936). Additionally, models based on habitat features also showed higher diagnostic AUCs compared to those based on whole TP features.

Furthermore, combined model of clinical indicators (age, sex, and KPS) and imaging indicators (habitat-based $nDDVD_{b0b10\_b10b20}$ and D) (model5) further significantly improved the diagnostic efficacy for IDH genotyping, achieving an AUC (95% CI) of 0.979 (0.953-1.000), with a sensitivity of 96.67% and specificity of 90.91%.

In order to better guide the image-based diagnosis, cut-off values of representative metrics and models under different diagnostic specificity for identifying IDH-wildtype gliomas were reported in Table 5.

Comparisons of AUCs for IDH genotyping

Assessments using the DeLong test showed that the improvement of AUC after habitat analysis was significant for $nDDVD_{b0b10}$ and f ($p=0.007$ and 0.009, respectively), but not significant for $DDVD_{b0b10\_b10b20}$, $DDVD_{b0b10}$, $nDDVD_{b0b10\_b10b20}$ and D ($p=0.219$, 0.054, 0.218 and 0.813, respectively). Compared to the best AUC of 0.763 from the whole TP, the best AUC of 0.823 from the tumor habitat showed a slight improvement ($p=0.218$), the AUC of the model3 improved significantly ($p=0.039$), and the model5 further significantly enhanced the AUC for IDH genotyping ($p<0.001$). In addition, compared to the AUCs of combined models of $nDDVD_{b0b10\_b10b20}$ and D (model1 and model3), the AUCs of combined models of f and D (model2 and model4) also improved slightly ($p=0.240$ and 0.375).

Table 2 Comparisons of DDVD and IVIM parameter values of whole TP between glioma groups

Metric	IDH-wildtype ($n=33$)	IDH-mutant ($n=30$)	Z	p	Glioblastoma ($n=28$)	Astrocytoma ($n=22$)	Oligodendroglioma ($n=8$)	Z	$p^{\#}$
DDVD									
$DDVD_{b0b10\_b10b20}$	14.48(12.93–18.60)	12.76(9.79–14.60)	-2.849	0.008**	14.22(13.07–18.38)	12.71(9.77–14.60)	12.76(10.50-15.21)	-2.697	0.014*
$DDVD_{b0b10}$	17.72(14.67–22.63)	17.89(13.58–20.83)	-1.046	0.296	17.94(14.72–22.52)	17.89(13.51–20.75)	17.53(15.10-21.75)	-1.075	0.282
$nDDVD_{b0b10\_b10b20}$	20.55(15.89–24.02)	15.14(11.61–19.29)	-3.578	< 0.001**	20.33(16.59–23.89)	15.26(11.41–19.29)	14.66(12.50-19.44)	-3.342	0.006**
$nDDVD_{b0b10}$	24.84(17.97–27.03)	21.10(16.09–25.24)	-1.830	0.080	24.15(18.64–26.55)	21.10(14.90-24.99)	19.82(17.17–27.20)	-1.759	0.119
IVIM									
IVIM_*D*	1.16(0.98–1.27)	1.31(1.19–1.39)	-3.358	0.003**	1.19(0.97–1.29)	1.32(1.18–1.40)	1.28(1.21–1.37)	-2.717	0.014*
IVIM_*f*	0.06(0.05–0.07)	0.05(0.03–0.06)	-1.830	0.080	0.06(0.05–0.07)	0.05(0.03–0.06)	0.05(0.04–0.06)	-1.368	0.205

Values are presented as median (interquartile range). Please note the *p* values were corrected for multiple comparisons using the Benjamini-Hochberg method. *$p<0.05$ and **$p<0.01$. Units for nDDVD and IVIM-D values are 10^{-3} and 10^{-3} mm^2/s, respectively. #represents the *p* value for comparison between glioblastoma and astrocytoma groups. DDVD = diffusion-derived vessel density, IVIM = intravoxel incoherent motion, TP = tumor parenchyma, IDH = isocitrate dehydrogenase

Correlations of Ki-67 LI with DDVD and IVIM values

The Ki-67 LI was significantly positively correlated with $DDVD_{b0b10\_b10b20}$ (rho = 0.437, $p<0.001$), $DDVD_{b0b10}$ (rho = 0.369, $p=0.005$), $nDDVD_{b0b10\_b10b20}$ (rho = 0.397, $p=0.002$), $nDDVD_{b0b10}$ (rho = 0.332, $p=0.010$), and *f* (rho = 0.456, $p<0.001$). Conversely, Ki-67 LI was significantly negatively correlated with *D* (rho = -0.262, $p=0.038$). After habitat analysis, the correlation coefficients improved from $-0.262\sim0.456$ based on whole TP features to $-0.551\sim0.516$ based on habitat features, as shown in Table 6.

Discussion

The current study is the first to apply DDVD in the investigation of brain gliomas. The current study showed that the DDVD values were significantly higher in IDH wild-type gliomas compared to IDH mutant gliomas, suggesting increased tissue micro-perfusion in the TP of IDH wild-type gliomas. Our findings are basically consistent with previous perfusion studies on gliomas [35, 36], in which significantly higher relative cerebral blood volume (rCBV) value was similarly found in IDH wild-type gliomas. According to the 2021 WHO classification of central nervous system tumors, glioblastomas constitute the majority of IDH wild-type gliomas. Pathologically, glioblastomas are characterized by two typical characteristics: microvascular proliferation and palisading necrosis [35, 37]. Therefore, the higher micro-perfusion observed in the TP of IDH wild-type gliomas can be attributed to the frequent occurrence of microvascular proliferation, which well explains the elevated DDVD values in these tumors.

The current study demonstrated that the Ki-67 LI was elevated in IDH-wildtype gliomas or glioblastomas and was positively correlated with DDVD. This suggests that an increased Ki-67 LI is linked to enhanced micro-perfusion in gliomas. The Ki-67 LI serves as an indicator of proliferating cells within a tumor, and a higher Ki-67 LI indicates greater proliferation [38]. It is a well-established biological principle that during periods of heightened cellular proliferation, there is a concomitant requirement for microvascular proliferation to ensure the supply of nutrients essential for cell growth. This concept is corroborated that a significantly higher microvascular density in glioblastomas with a Ki-67 LI exceeding 20% [39]. This explains why a higher Ki-67 LI was correlated with higher DDVD values. Notably, our recent study with endometrial carcinoma also showed Ki-67 high-proliferation or aggressive histological type had higher DDVD value than those with Ki-67 low-proliferation or non-aggressive histological type [27].

It is noteworthy that the present study observed a relatively better performance of $DDVD_{b0b10\_b10b20}$ compared to $DDVD_{b0b10}$ in both IDH genotyping and Ki-67

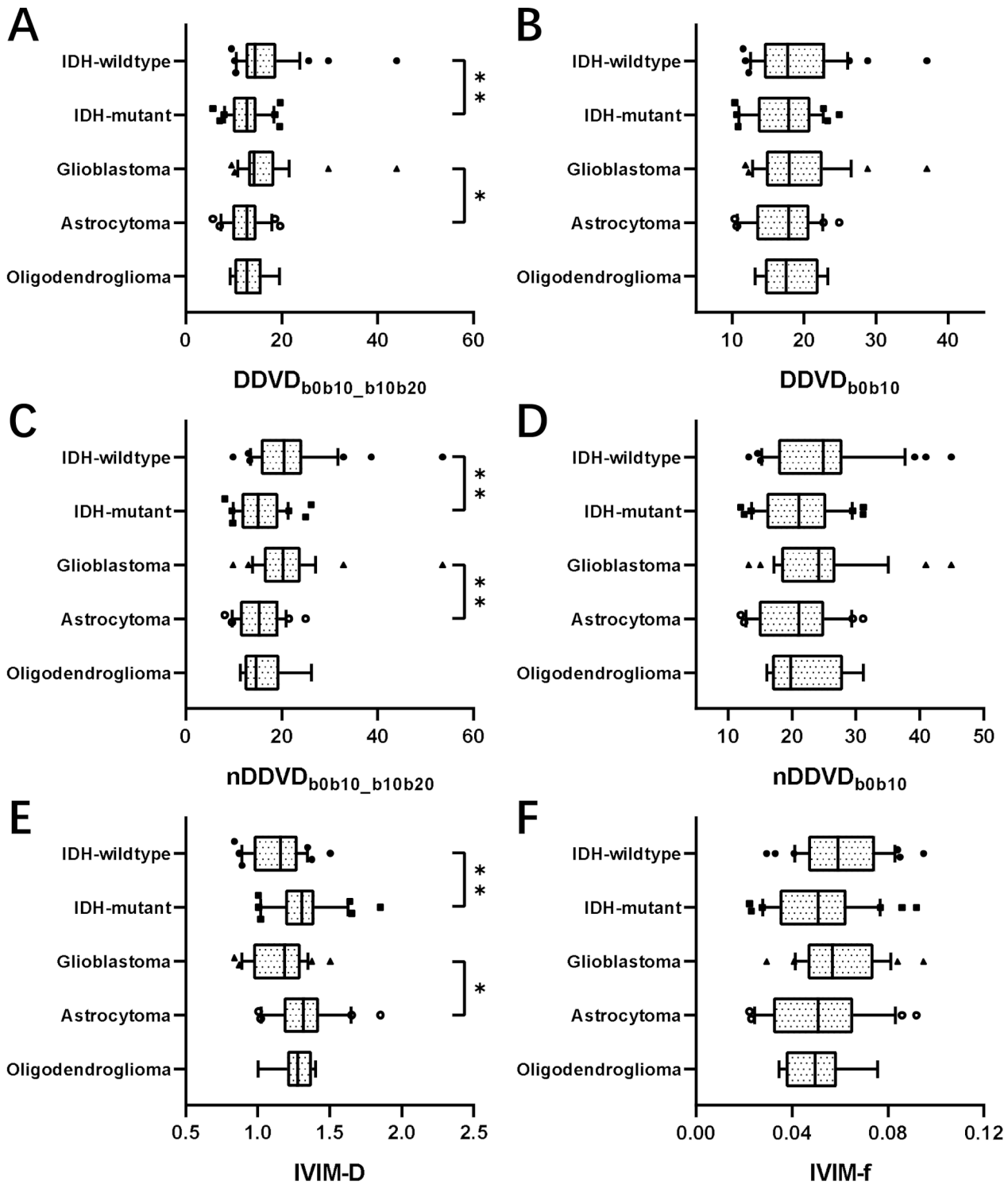

Fig. 3 Box and whisker graphs for separating IDH genotypes and tumor subtypes. Box and whisker graphs show distributions of $DDVD_{b0b10\_b10b20}$ (**A**), $DDVD_{b0b10}$ (**B**), $nDDVD_{b0b10\_b10b20}$ (**C**), $nDDVD_{b0b10}$ (**D**), IVIM_*D* (**E**), IVIM_*f* (**F**) values of the whole TP that could be used to identify the IDH genotype and tumor subtype of adult-type diffuse gliomas. * $p < 0.05$ and ** $p < 0.01$. TP = tumor parenchyma, IDH = isocitrate dehydrogenase, DDVD = diffusion-derived vessel density, IVIM = intravoxel incoherent motion

Table 3 Diagnostic performance of DDVD and IVIM parameter values for IDH genotyping of gliomas

Region/Metrics		$DDVD_{b0b10\_b10b20}$		$DDVD_{b0b10}$		$nDDVD_{b0b10\_b10b20}$		$nDDVD_{b0b10}$		IVIM_D		IVIM_f	
		AUC	*p*	AUC	*p*	AUC	*p*	AUC	*p*	AUC	*p*	AUC	*p*
Whole TP		**0.709**	0.008**	0.577	0.296	**0.763**	<0.001**	0.634	0.080	**0.746**	0.003**	0.634	0.080
Tumor habitat													
$DDVD_{b0b10\_b10b20}$	Mask1	0.559	0.510	0.588	0.356	0.693	0.027*	0.501	0.989	0.746	0.006**	0.587	0.356
	Mask2	0.751	0.002**	0.615	0.117	0.804	<0.001**	0.712	0.005**	0.735	0.002**	0.711	0.005**
$DDVD_{b0b10}$	Mask1	0.727	0.004**	0.587	0.284	0.765	<0.001**	0.562	0.401	0.744	0.003**	0.597	0.279
	Mask2	**0.785**	<0.001**	**0.731**	0.002**	**0.823**	<0.001**	**0.809**	<0.001**	0.746	0.001**	**0.779**	<0.001**
$nDDVD_{b0b10\_b10b20}$	Mask1	0.566	0.445	0.588	0.347	0.638	0.177	0.535	0.630	0.741	0.006**	0.592	0.347
	Mask2	0.690	0.015*	0.594	0.201	0.799	<0.001**	0.672	0.023*	0.735	0.003**	0.704	0.010*
$nDDVD_{b0b10}$	Mask1	0.621	0.149	0.642	0.104	0.729	0.006**	0.560	0.417	0.726	0.006**	0.604	0.187
	Mask2	0.731	0.003**	0.626	0.085	0.808	<0.001**	0.769	<0.001**	0.739	0.002**	0.719	0.004**
IVIM_*D*	Mask1	0.722	0.004**	0.612	0.127	0.737	0.003**	0.641	0.081	**0.760**	<0.001**	0.619	0.125
	Mask2	0.678	0.030*	0.585	0.298	0.692	0.027*	0.600	0.260	0.519	0.799	0.710	0.024*
IVIM_*f*	Mask1	0.576	0.513	0.570	0.513	0.680	0.042*	0.531	0.670	0.721	0.018*	0.532	0.670
	Mask2	0.696	0.016*	0.571	0.335	0.697	0.016*	0.618	0.161	0.732	0.012*	0.608	0.169

Please note the *p* values were corrected for multiple comparisons using the Benjamini-Hochberg method. *$p<0.05$ and **$p<0.01$. DDVD = diffusion-derived vessel density, IVIM = intravoxel incoherent motion, TP = tumor parenchyma, IDH = isocitrate dehydrogenase, AUC = area under curve

correlation analysis. The improved performance of $DDVD_{b0b10\_b10b20}$ may be attributed to its design, which subtracts the b10b20 element from b0b10, thereby reducing the diffusion component present in $DDVD_{b0b10}$ [15, 28]. This study also applied habitat analysis. Tumor cells have different genetic traits in different areas of the tumor. This means a tumor is like a mix of different environments, each with its own conditions and cell behaviors. These differences cause tumor cells to interact with their surroundings, leading to genetic changes in the tumor [31]. A habitat imaging method can use MR images to create a set of phenotypic heterogeneity maps showing these differences, which can help in identifying representative subregions of tumor [40, 41]. In the current study, the diagnostic efficiency was significantly improved for DDVD, *D*, and *f* values in classifying IDH genotypes through habitat analysis and the correlation of these parameter values with Ki-67 LI was also enhanced. This improvement is likely because habitat analysis effectively identifies representative subregions of gliomas. Of note, the most notable improvements were observed in the metric values derived from the habitats with higher DDVD value and lower *D* value, which represent subregions with higher malignancy in gliomas.

In this study, the modeling analysis revealed that the diagnostic efficiency of the combined model using DDVD and *D* was superior to that using *f* and *D* for IDH genotyping, suggesting that DDVD might provide a more accurate assessment of micro-perfusion compared to IVIM_*f* of IVIM. As expected, predictive models based on habitat features demonstrated better diagnostic performance than those based on the whole TP features. When clinical indicators (age, sex, and KPS) were further integrated into a model, the diagnostic efficacy for IDH genotyping was further improved.

There were some limitations in this study. First, it used a single-center study with a relatively small sample size, especially for patients with oligodendroglioma. Second, DWI scan parameters can be further optimized. The second *b*-value of 10 s/mm^2 was relatively high for DDVD analysis. Our earlier study showed that $DDVD_{b0b2}$ is better in assessing HCC than $DDVD_{b0b10}$ [12, 18], which is consistent with the initial definition of DDVD [14]. The NEX of DWI in this study was only 1. Our recent experience shows increasing NEX can improve DDVD measure stability, and since the DDVD protocol is very fast, higher NEX will be practically feasible. Moreover, tumor habitats defined based on diffusion MRI using otsu method clustering into higher and lower value habitats could not be confirmed pathologically. However, such a pathological correlation would be challenging to achieve. Future studies with more optimized DWI scan parameters and with larger sample sizes for various types of gliomas are highly desirable. Another limitation is that follow-up

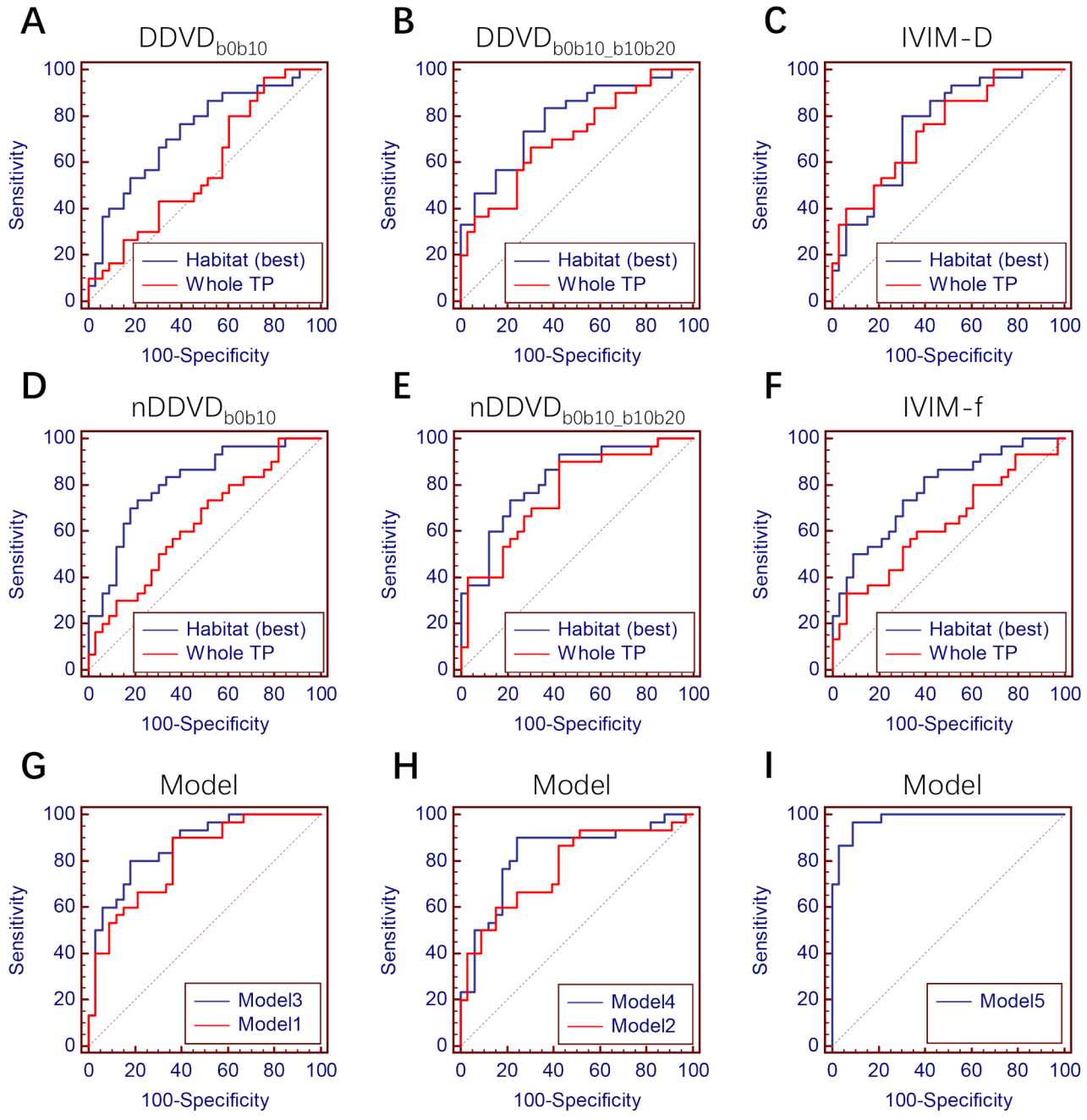

Fig. 4 ROC curves for DDVD and IVIM parameters and models when separating IDH genotypes of gliomas. ROC curves for $DDVD_{b0b10}$ (**A**), $DDVD_{b0b10\_b10b20}$ (**B**), IVIM_*D* (**C**), $nDDVD_{b0b10}$ (**D**), $nDDVD_{b0b10\_b10b20}$ (**E**), IVIM_*f* (**F**) values of the whole TP and their best habitats, and models reported in Table 4 (**G**, **H**, **I**) when distinguishing IDH-wildtype gliomas from IDH-mutant gliomas. AUC = area under the curve, TP = tumor parenchyma, IDH = isocitrate dehydrogenase, DDVD = diffusion-derived vessel density, IVIM = intravoxel incoherent motion

imaging of the patients was unavailable to us, thus we could not assess the correlation between DDVD measures with the glioma recurrence rate.

In conclusion, DDVD, an in vivo measure of vessel micro-perfusion, can help to distinguish between IDH genotypes in diffuse gliomas. Habitat analysis enhances the performance of DDVD for IDH genotyping and Ki-67 evaluation. These findings suggest that DDVD can serve as a novel biomarker for IDH genotyping in adult-type diffuse gliomas, aiding in personalized treatment strategies and probably also in post-treatment follow-ups.

Table 4 Modeling and evaluating diagnostic performance of models for IDH genotyping of gliomas

Model	β	*p*	AUC (95%CI)	Sen/Spe (%)
Imaging model				
Whole TP feature				
Model1			0.812 (0.708–0.917)	90.00/63.64
$nDDVD_{b0b10\_b10b20}$ #	-0.152	0.017*		
IVIM_*D*#	4.662	0.012*		
Constant	-2.999	0.253		
Model2			0.774 (0.656–0.892)	60.00/84.85
IVIM_*f*#	-31.537	0.071		
IVIM_*D*#	5.643	0.002**		
Constant	-5.187	0.023		
Habitat feature				
Model3			0.866 (0.777–0.954)	80.00/81.82
$nDDVD_{b0b10\_b10b20}$ ##	-0.119	0.004**		
IVIM_*D*##	10.243	0.010*		
Constant	-7.310	0.109		
Model4			0.828 (0.721–0.936)	90.00/75.76
IVIM_*f*##	-47.403	0.011*		
IVIM_*D*##	8.387	0.024*		
Constant	-4.722	0.304		
Clinical + imaging model				
Model5			0.979 (0.953-1.000)	96.67/90.91
Age	-0.354	0.009**		
Sex	-3.193	0.052		
KPS	0.108	0.026*		
$nDDVD_{b0b10\_b10b20}$ ##	-0.239	0.006**		
IVIM_*D*##	28.171	0.018*		
Constant	-13.891	0.114		

*$p<0.05$ and **$p<0.01$. # represents features from Whole TP and ## represents features from Habitat. IDH = isocitrate dehydrogenase, AUC = area under curve, CI = confidence interval, TP = tumor parenchyma, DDVD = diffusion-derived vessel density, IVIM = intravoxel incoherent motion, KPS = Karnofsky performance status

Table 5 Cut-off values of representative metrics and models under different diagnostic specificity for identifying IDH-wildtype gliomas

Metric	Specificity					
	75%	**80%**	**85%**	**90%**	**95%**	**100%**
$nDDVD_{b0b10\_b10b20}$ #	19.267	19.304	19.327	19.636	24.911	26.185
IVIM-*D*#	1.191	1.173	1.160	1.021	1.005	0.983
$nDDVD_{b0b10\_b10b20}$ ##	28.985	29.776	31.466	32.904	36.343	48.671
IVIM-*D*##	1.071	1.055	1.019	1.003	0.975	0.882
Model3	0.550	0.536	0.292	0.268	0.185	0.104
Model5	0.831	0.785	0.714	0.472	0.351	0.142

Units for nDDVD and IVIM-D values are 10^{-3} and 10^{-3} mm^2/s, respectively. # represents features from Whole TP and ## represents features from Habitat. IDH = isocitrate dehydrogenase, DDVD = diffusion-derived vessel density, IVIM = intravoxel incoherent motion

Table 6 Correlation of Ki-67 LI with DDVD and IVIM parameters in whole TP and habitats

Region/Metrics		$DDVD_{b0b10\_b10b20}$		$DDVD_{b0b10}$		$nDDVD_{b0b10\_b10b20}$		$nDDVD_{b0b10}$		IVIM_D		IVIM_f	
		rho	*p*	rho	*p*	rho	*p*	rho	*p*	rho	*p*	rho	*p*
Whole TP		**0.437**	< 0.001**	**0.369**	0.005**	**0.397**	0.002**	**0.332**	0.010*	**-0.262**	0.038*	**0.456**	< 0.001**
Tumor habitat													
$DDVD_{b0b10\_b10b20}$	Mask1	0.310	0.028*	0.237	0.061	0.311	0.028*	0.245	0.061	-0.248	0.061	0.442	< 0.001**
	Mask2	0.376	0.004**	0.393	0.003**	0.360	0.005**	0.368	0.005**	-0.185	0.146	0.497	< 0.001**
$DDVD_{b0b10}$	Mask1	0.251	0.071	0.177	0.164	0.311	0.026*	0.231	0.083	-0.336	0.021*	0.416	0.006**
	Mask2	0.232	0.080	0.357	0.012*	0.267	0.053	0.299	0.034*	-0.166	0.193	0.445	< 0.001**
$nDDVD_{b0b10\_b10b20}$	Mask1	0.255	0.061	0.266	0.061	0.342	0.018*	0.246	0.061	-0.226	0.075	0.456	< 0.001**
	Mask2	0.291	0.025*	0.342	0.009**	0.392	0.004**	0.380	0.004**	-0.249	0.049*	0.501	< 0.001**
$nDDVD_{b0b10}$	Mask1	0.163	0.303	0.126	0.324	0.272	0.062	0.130	0.324	-0.292	0.060	0.421	0.006**
	Mask2	0.287	0.028*	0.353	0.010*	0.339	0.011*	**0.410**	0.003**	-0.199	0.118	**0.516**	< 0.001**
IVIM_*D*	Mask1	0.406	0.002**	0.362	0.004**	0.377	0.003**	0.357	0.004**	**-0.551**	< 0.001**	0.442	< 0.001**
	Mask2	**0.442**	< 0.001**	**0.405**	0.002**	**0.394**	0.002**	0.304	0.018*	0.230	0.069	0.470	< 0.001**
IVIM_*f*	Mask1	0.227	0.111	0.101	0.431	0.292	0.060	0.117	0.431	-0.314	0.060	0.251	0.096
	Mask2	0.234	0.194	0.170	0.218	0.211	0.194	0.120	0.350	-0.190	0.204	0.333	0.048*

Please note the *p* values were corrected for multiple comparisons using the Benjamini-Hochberg method. * $p < 0.05$ and ** $p < 0.01$. Ki-67 LI = Ki-67 labeling index, DDVD = diffusion-derived vessel density, IVIM = intravoxel incoherent motion, TP = tumor parenchyma

Abbreviations

DWI	Diffusion-weighted imaging
IDH	Isocitrate dehydrogenase
TP	Tumor parenchyma
DDVD	Diffusion-derived vessel density
IVIM	Intravoxel incoherent motion
AUC	Area under curve
ROC	Receiver operating characteristic
ROI	Region of interest
WHO	World Health Organization
CNS	Central nervous system
TERT	Telomerase reverse transcriptase
EGFR	Epidermal growth factor receptor
NEC	Not elsewhere classified
KPS	Karnofsky performance status
T1-mprage	T1-weighted magnetization prepared rapid gradient echo sequence
T2WI	T2-weighted imaging
FSE	Fast spin-echo
FLAIR	Fluid attenuated inversion recovery
Ki-67 LI	Ki-67 labeling index
PCR	Polymerase chain reaction
ICC	Intra-class correlation coefficient

Supplementary Information

The online version contains supplementary material available at https://doi.org/10.1186/s12880-025-01605-4.

Supplementary Material 1

Acknowledgements

The authors thank Yifan Sun from Fujian Medical University Union Hospital for her invaluable contributions to the tumor segmentation process.

Author contributions

RF Jiang and YXJ Wáng contributed to the design and implementation of the research. CX Ni, RL Lin, DQ Yao, FZ Ma, Y Song and G Yang contributed to the analysis of the results and writing of the manuscript. RL Lin, YY He and YT Shi participated in the data collection. All authors read and approved the final version of the manuscript.

Funding

This work was funded by the grants from Joint Funds for the innovation of science and Technology, Fujian province (2021Y9055), and the Science and Technology Plan Project of Fujian Health Commission (2022GGA013).

Data availability

The datasets used and analysed during the current study are available from the corresponding author upon reasonable request.

Declarations

Ethics approval and consent to participate

Ethical approval was granted by the Ethics Committee of Fujian Medical University Union Hospital, and all participants provided informed consent. All methods were carried out according to relevant guidelines and regulations.

Consent for publication

Not applicable.

Clinical trial number

not applicable.

Competing interests

Yang Song is an employee of Siemens Healthineers Ltd. Shanghai, China. Yì Xiáng J. Wáng is the founder of Yingran Medicals Ltd., which develops medical image-based diagnostics software. Other authors declare no conflict of interest.

Author details
[1]Department of Radiology, Fujian Medical University Union Hospital, NO.29 Xinquan Road, Fuzhou 350001, Fujian, P. R. China
[2]Department of Imaging and Interventional Radiology, Faculty of Medicine, The Chinese University of Hong Kong, Shatin, New Territories, Hong Kong SAR, China
[3]MR Research Collaboration Team, Siemens Healthineers Ltd., Shanghai, China
[4]Shanghai Key Laboratory of Magnetic Resonance, East China Normal University, Shanghai 200062, China
[5]School of Medical Imaging, Fujian Medical University, Fuzhou 350004, China

Received: 25 October 2024 / Accepted: 19 February 2025
Published online: 06 March 2025

References

1. Louis DN, Perry A, Wesseling P, Brat DJ, Cree IA, Figarella-Branger D, et al. The 2021 WHO classification of tumors of the central nervous system: a summary. Neuro Oncol. 2021;23:1231–51.
2. Lee S, Choi SH, Ryoo I, Yoon TJ, Kim TM, Lee SH, et al. Evaluation of the microenvironmental heterogeneity in high-grade gliomas with IDH1/2 gene mutation using histogram analysis of diffusion-weighted imaging and dynamic-susceptibility contrast perfusion imaging. J Neurooncol. 2015;121(1):141–50.
3. Shen N, Zhao L, Jiang J, Jiang R, Su C, Zhang S, Tang X, Zhu W. Intravoxel incoherent motion diffusion-weighted imaging analysis of diffusion and microperfusion in grading gliomas and comparison with arterial spin labeling for evaluation of tumor perfusion. J Magn Reson Imaging. 2016;44:620–32.
4. Wáng YXJ, Ma FZ. A tri-phasic relationship between T2 relaxation time and magnetic resonance imaging (MRI)-derived apparent diffusion coefficient (ADC). Quant Imaging Med Surg. 2023;13:8873–80.
5. Wang X, Cao M, Chen H, Ge J, Suo S, Zhou Y. Simplified perfusion fraction from diffusion-weighted imaging in preoperative prediction of IDH1 mutation in WHO grade II-III gliomas: comparison with dynamic contrast-enhanced and intravoxel incoherent motion MRI. Radiol Oncol. 2020;54:301–10. d.
6. Wang X, Chen XZ, Shi L, Dai JP. Glioma grading and IDH1 mutational status: assessment by intravoxel incoherent motion MRI. Clin Radiol. 2019;74:e6517–65114.
7. Federau C, Cerny M, Roux M, Mosimann PJ, Maeder P, Meuli R, et al. IVIM perfusion fraction is prognostic for survival in brain glioma. Clin Neuroradiol. 2017;27:485–92.
8. Keil VC, Mädler B, Gielen GH, Pintea B, Hiththetiya K, Gaspranova AR, et al. Intravoxel incoherent motion MRI in the brain: impact of the fitting model on perfusion fraction and lesion differentiability. J Magn Reson Imaging. 2017;46:1187–99.
9. Wang YXJ, Huang H, Zheng CJ, Xiao BH, Chevallier O, Wang W. Diffusion-weighted MRI of the liver: challenges and some solutions for the quantification of apparent diffusion coefficient and intravoxel incoherent motion. Am J Nucl Med Mol Imaging. 2021;11:107–42.
10. Wáng YXJ. A reduction of perfusion can lead to an artificial elevation of slow diffusion measure: examples in acute brain ischemia MRI intravoxel incoherent motion studies. Ann Transl Med. 2021;9:895.
11. Wáng YXJ. Observed Paradoxical perfusion fraction elevation in steatotic liver: an example of intravoxel incoherent motion modeling of the perfusion component constrained by the diffusion component. NMR Biomed. 2021;34:e4488.
12. Li XM, Yao DQ, Quan XY, Li M, Chen W, Wáng YXJ. Perfusion of hepatocellular carcinomas measured by diffusion-derived vessel density biomarker: higher hepatocellular carcinoma perfusion than earlier intravoxel incoherent motion reports. NMR Biomed. 2024;37:e5125.
13. Ma FZ, Wáng YXJ. *T2* relaxation time elongation of hepatocellular carcinoma relative to native liver tissue leads to an underestimation of perfusion fraction measured by standard intravoxel incoherent motion magnetic resonance imaging. Quant Imaging Med Surg. 2024;14:1316–22.
14. Wáng YXJ. Living tissue intravoxel incoherent motion (IVIM) diffusion MR analysis without $b=0$ image: an example for liver fibrosis evaluation. Quant Imaging Med Surg. 2019;9:127–33.
15. Ma FZ, Xiao BH, Wáng YXJ. MRI signal simulation of liver DDVD (diffusion derived 'vessel density') with multiple compartments diffusion model. Quant Imaging Med Surg. 2025;15:1710–8.
16. Huang H, Zheng CJ, Wang LF, Che-Nordin N, Wáng YXJ. Age and gender dependence of liver diffusion parameters and the possibility that intravoxel incoherent motion modeling of the perfusion component is constrained by the diffusion component. NMR Biomed. 2021;34:e4449.
17. He J, Chen C, Xu L, Xiao B, Chen Z, Wen T. Diffusion-Derived vessel density computed from a simplified intravoxel incoherent motion imaging protocol in pregnancies complicated by early preeclampsia: A novel biomarker of placental dysfunction. Hypertension. 2023;80:1658–67.
18. Li CY, Chen L, Ma FZ, Chen JQ, Zhan YF, Wáng YXJ. High performance of the diffusion magnetic resonance imaging biomarker diffusion-derived 'vessel density' (DDVD) for separating placentas associated with pre-eclampsia from placentas in normal pregnancy. Quant Imaging Med Surg. 2025;15:1–14.
19. Lu T, Wang L, Li M, Wang Y, Chen M, Xiao BH, et al. Diffusion-derived vessel density (DDVD) computed from a simple diffusion MRI protocol as a biomarker of placental blood circulation in patients with placenta accreta spectrum disorders: A proof-of-concept study. Magn Reson Imaging. 2024;109:180–6.
20. Hu GW, Li CY, Zhang G, Zheng CJ, Ma FZ, Quan XY, et al. Diagnosis of liver hemangioma using magnetic resonance diffusion-derived vessel density (DDVD) pixelwise map: a preliminary descriptive study. Quant Imaging Med Surg. 2024;14:8064–82.
21. Chen JQ, Li CY, Wang W, Yao DQ, Jiang RF, Wáng YXJ. Diffusion-derived vessel density (DDVD) for penumbra delineation in acute ischemic stroke: initial proof-of-concept results using single NEX DWI. Quant Imaging Med Surg. 2024;14:9533–954.
22. Sahani DV, Holalkere NS, Mueller PR, Zhu AX. Advanced hepatocellular carcinoma: CT perfusion of liver and tumor tissue–initial experience. Radiology. 2007;243:736–43.
23. Ippolito D, Capraro C, Casiraghi A, Cestari C, Sironi S. Quantitative assessment of tumour associated neovascularisation in patients with liver cirrhosis and hepatocellular carcinoma: role of dynamic-CT perfusion imaging. Eur Radiol. 2012;22:803–11.
24. Lu BL, Yao DQ, Wáng YXJ, Zhang ZW, Wen ZQ, Xiao BH, et al. Higher perfusion of rectum carcinoma relative to tumor-free rectal wall: quantification by a new imaging biomarker diffusion-derived vessel density (DDVD). Quant Imaging Med Surg. 2024;14:3264–74.
25. Xu Y, Sun H, Song A, Yang Q, Lu X, Wang W. Predictive significance of tumor grade using 256-Slice CT Whole-Tumor perfusion imaging in colorectal adenocarcinoma. Acad Radiol. 2015;22:1529–35.
26. Hayano K, Shuto K, Koda K, Yanagawa N, Okazumi S, Matsubara H. Quantitative measurement of blood flow using perfusion CT for assessing clinicopathologic features and prognosis in patients with rectal cancer. Dis Colon Rectum. 2009;52:1624–9.
27. Wang F, Wang Y, Qi L, Liang J, Xiao BH, Zhang C, et al. High correlation between Ki-67 expression and a novel perfusion MRI biomarker diffusion-derived vessel density (DDVD) in endometrial carcinoma. Magn Reson Imaging. 2025;117:110324. https://doi.org/10.1016/j.mri.2025.110324
28. Yao DQ, Zheng CJ, Deng YY, Lu BL, Lu T, Hu GW, et al. Potential diverse applications of diffusion-derived vessel density (DDVD) pixel-by-pixel mapping. Quant Imaging Med Surg. 2024;14:2136–45.
29. Tamma R, Ingravallo G, Annese T, d'Amati A, Lorusso L, Ribatti D. Tumor microenvironment and microvascular density in human glioblastoma. Cells. 2022;12:11.
30. Liu M, Ji Z, Jain V, Smith VL, Hocke E, Patel AP, et al. Spatial transcriptomics reveals segregation of tumor cell States in glioblastoma and marked immunosuppression within the perinecrotic niche. Acta Neuropathol Commun. 2024;12:64.
31. Gatenby RA, Grove O, Gillies RJ. Quantitative imaging in cancer evolution and ecology. Radiology. 2013;269:8–15.
32. Kim JY, Gatenby RA. Quantitative clinical imaging methods for monitoring intratumoral evolution. Methods Mol Biol. 2017;1513:61–81.
33. Kim M, Park JE, Kim HS, Kim N, Park SY, Kim YH, et al. Spatiotemporal habitats from multiparametric physiologic MRI distinguish tumor progression from treatment-related change in post-treatment glioblastoma. Eur Radiol. 2021;31:6374–83.
34. Lee DH, Park JE, Kim N, Park SY, Kim YH, Cho YH, et al. Tumor habitat analysis by magnetic resonance imaging distinguishes tumor progression from radiation necrosis in brain metastases after stereotactic radiosurgery. Eur Radiol. 2022;32:497–507.

35. Siakallis L, Topriceanu CC, Panovska-Griffiths J, Bisdas S. The role of DSC MR perfusion in predicting IDH mutation and 1p19q codeletion status in gliomas: meta-analysis and technical considerations. Neuroradiology. 2023;65(7):1111–26.
36. Cindil E, Sendur HN, Cerit MN, Erdogan N, Celebi F, Dag N, et al. Prediction of IDH mutation status in high-grade gliomas using DWI and high T1-weight DSC-MRI. Acad Radiol. 2022;29(Suppl 3):S52–62.
37. Alexiou GA, Zikou A, Tsiouris S, Goussia A, Kosta P, Papadopoulos A, et al. Correlation of diffusion tensor, dynamic susceptibility contrast MRI and (99m) Tc-Tetrofosmin brain SPECT with tumour grade and Ki-67 immunohistochemistry in glioma. Clin Neurol Neurosurg. 2014;116:41–5.
38. Fisher BJ, Naumova E, Leighton CC, Naumov GN, Kerklviet N, Fortin D, et al. Ki-67: a prognostic factor for low-grade glioma? Int J Radiat Oncol Biol Phys. 2002;52:996–1001.
39. Sipos TC, Kövecsi A, Kocsis L, Nagy-Bota M, Pap Z. Evaluation of microvascular density in glioblastomas in relation to p53 and Ki67 Immunoexpression. Int J Mol Sci. 2024;25:6810.
40. Swanton C. Intratumor heterogeneity: evolution through space and time. Cancer Res. 2012;72:4875–82.
41. Wu H, Tong H, Du X, Guo H, Ma Q, Zhang Y, et al. Vascular habitat analysis based on dynamic susceptibility contrast perfusion MRI predicts IDH mutation status and prognosis in high-grade gliomas. Eur Radiol. 2020;30:3254–65.

Publisher's note